



CCL21-loaded 3D hydrogels for T cell expansion and differentiation

Eduardo Pérez del Río ^{a,b}, Fabião Santos ^a, Xavier Rodriguez Rodriguez ^{a,c}, Marc Martínez-Miguel ^{a,c}, Ramon Roca-Pinilla ^d, Anna Arís ^d, Elena Garcia-Fruitós ^d, Jaume Veciana ^{a,b}, Joachim P. Spatz ^{e,f}, Imma Ratera ^{a,b,**}, Judith Guasch ^{a,b,c,*}

^a Institute of Materials Science of Barcelona (ICMAB-CSIC), Campus UAB, Bellaterra, 08193, Spain

^b Networking Research Center on Bioengineering, Biomaterials and Nanomedicine (CIBER-BBN), Campus UAB, Bellaterra, 08193, Spain

^c Dynamic Biomimetics for Cancer Immunotherapy, Max Planck Partner Group, ICMAB-CSIC, Campus UAB, Bellaterra, 08193, Spain

^d Department of Ruminant Production, Institut de Recerca i Tecnologia Agroalimentàries (IRTA), Caldes de Montbui, 08140, Spain

^e Max Planck Institute for Medical Research, Jahnstraße 29, Heidelberg, 69120, Germany

^f Institute for Physical Chemistry, Heidelberg University, INF 253, Heidelberg, 69120, Germany

ARTICLE INFO

Keywords:
3D hydrogels
T cells
Cytokines
Proliferation
Lymph nodes
Adoptive cell therapy

ABSTRACT

Recent achievements in the field of immunotherapy, such as the development of engineered T cells used in adoptive cell therapy, are introducing more efficient strategies to combat cancer. Nevertheless, there are still many limitations. For example, these T cells are challenging to manufacture, manipulate, and control. Specifically, there are limitations in producing the large amounts of therapeutic T cells needed for these therapies in a short period of time and in an economically viable manner. In this study, three-dimensional (3D) poly(ethylene) glycol (PEG) hydrogels covalently combined with low molecular weight heparin are engineered to resemble the lymph nodes, where T cells reproduce. In these hydrogels, PEG provides the needed structural and mechanical properties, whereas heparin is used as an anchor for the cytokine CCL21, which is present in the lymph nodes, and can affect cell migration and proliferation. The 3D structure of the hydrogel in combination with its loading capacity result in an increased primary human CD4⁺ T cell proliferation compared to the state-of-the-art expansion systems consisting of artificial antigen presenting cells. Thus, we present a new tool for adoptive cell therapy to help achieving the large numbers of cells required for therapy of selected phenotypes targeted against cancer cells, by mimicking the lymph nodes.

1. Introduction

Immunotherapy is a medical strategy that offers an approach different from chemotherapy, radiation, and surgery in the treatment of cancer, which is based on harnessing the immune system of patients. The immune system protects the organism against disease, distinguishing between self and non-self. Nevertheless, cancer appears from the own cells of an organism, and it creates a tumor microenvironment with immune evasion and immunosuppression signals capable of avoiding the immune response [1]. Fortunately, T cells can be genetically modified by engineering their T cell receptors (TCRs) or making them express chimeric antigen receptors (CARs) to recognize and eliminate malignant cells more effectively [2]. These cells have been used in adoptive cell therapy (ACT), resulting in some encouraging achievements [3]. Indeed, the use of living cells as therapeutic agents is radically different from

other available systems such as small molecules or antibodies due to the capacity of cells to sense and develop different responses depending on the stimulus that they are exposed to. Nonetheless, this therapy is technically challenging [4], i.e. modified T cells are difficult to manufacture, manipulate, and control [5]. Specifically, the efficiency of the *ex vivo* expansion process of these functional T cells to achieve relevant clinical doses is a major limiting factor to translate the therapy to clinics [2]. Additionally, ACT based on tumor infiltrating lymphocytes (TILs) [6,7], which are T cells that infiltrate a tumor and are selective for it, would also benefit from efficient expansion systems, due to their low prevalence [8].

Although different approaches have been proposed [9,10], including materials with control at the nanoscale [11–15], *ex vivo* T cell expansions are usually performed in suspension using artificial antigen presenting cells (APCs), such as Dynabeads® (Thermo Fisher Scientific,

* Corresponding author. Institute of Materials Science of Barcelona (ICMAB-CSIC), Campus UAB, Bellaterra, 08193, Spain.

** Corresponding author. Institute of Materials Science of Barcelona (ICMAB-CSIC), Campus UAB, Bellaterra, 08193, Spain.

E-mail addresses: iratera@icmab.es (I. Ratera), jguasch@icmab.es (J. Guasch).

USA). These artificial beads are 4.5 μm superparamagnetic spheres decorated with the antibodies antiCD3 and antiCD28, which polyclonally activate T cells through the TCR complex and the costimulating receptor CD28 [16–19], thus mimicking the natural immunological synapse. However, the secondary lymphoid organs (SLOs), especially the lymph nodes (LNs), where the interaction between these cells occurs in our body, are not considered despite the growing evidence of their influence [20–22]. For example, the LNs provide homing signals through the cytokine CCL21, which is immobilized in the lymphoid tissues through its extended C terminus that reversibly binds to glycosaminoglycan components of the extracellular matrix (ECM), namely heparan sulfate [23,24]. CCL21 interacts with naïve T cells and APCs, through the chemokine receptor CCR7, enhancing CD4 $^{+}$ and CD8 $^{+}$ T cell proliferation and promoting random migration [25,26].

Hydrogels are three-dimensional (3D) natural or synthetic structures that are often used as a tool to mimic the ECM with the objective to recreate the natural environment of cells [27–29]. These systems offer more realistic conditions than hard planar substrates such as standard polystyrene dishes, improving the standard cell culture techniques [30]. They can also be used to put cells in contact with different proteins and growth factors, which can influence different cellular responses, such as differentiation or growth [31]. Poly(ethylene glycol) (PEG) hydrogels have been extensively studied because of their interesting physicochemical properties, such as their tunable stiffness, which can be varied over six orders of magnitude [32]. These hydrogels are biologically inert due to their hydrophilic character, which prevents unspecific attachment to proteins, but they have shown to successfully encapsulate cells with maintained cell viability, even without integrin-binding ligands [33,34]. Nevertheless, they can be easily engineered to present different functionalities such as cell adhesive motifs [35–37]. Moreover, they can be manufactured under mild and cyocompatible conditions with high reproducibility [38,39].

Heparin is a common anticoagulant used to prevent the formation of blood clots as well as to treat venous thromboembolisms and myocardial infarction, based on its capacity to interact with positively charged

binding sites of proteins [40]. Indeed, heparin can be neutralized in case of an adverse clinical effect with protamine, a small protein rich in the positively charged amino acid arginine at physiological pH [41]. The anionic charge of heparin has also been exploited to improve its absorption with positively charged polyethylenimines [42]. In fact, heparin is described as a more sulfated variant of heparan, which can bind to different proteins such as CCL21, through its anionic character as well as sequence specificity in some cases [31,43]. Low molecular weight heparin (LMWH) offers some advantages over unfractionated heparin (UFH) in clinical settings such as a subcutaneous delivery, reduced risk of hemorrhage, longer half-life, greater bioavailability, and more predictable pharmacokinetics [44]. Moreover, its smaller size and lower polydispersity compared to UFH [45,46], promote hydrogel reproducibility, as previously shown for PEG-LMWH hydrogels [47,48].

Here we describe a family of 3D hydrogels consisting of PEG and LMWH (PEG-Hep hydrogels) loaded with CCL21 that were synthesized and fully characterized in order to imitate the conditions of the ECM of the LNs with the objective to increase primary human (CD4 $^{+}$) T cell proliferation and tune differentiation for ACT (Fig. 1).

CD4 $^{+}$ T cell proliferation was enhanced when using these 3D structures in combination to the artificial APCs Dynabeads, thus improving the state-of-the-art suspension systems. Additionally, the phenotypes obtained – naïve (T_N), central memory (T_{CM}), and effector memory (T_{EM}) – were studied given their clinical importance.

2. Results and discussion

2.1. Synthesis and characterization of PEG-Hep hydrogels

In this section, the synthesis of PEG-Hep hydrogels is provided, which is based on previous reports [47,48]. Moreover, we describe the capacity of these hydrogels to be loaded with proteins through the heparin unit, mostly through electrostatic interactions, as it has been shown for other systems [49]. Indeed, the protein repellent character of PEG prevents unspecific interactions, thus resulting in well-defined

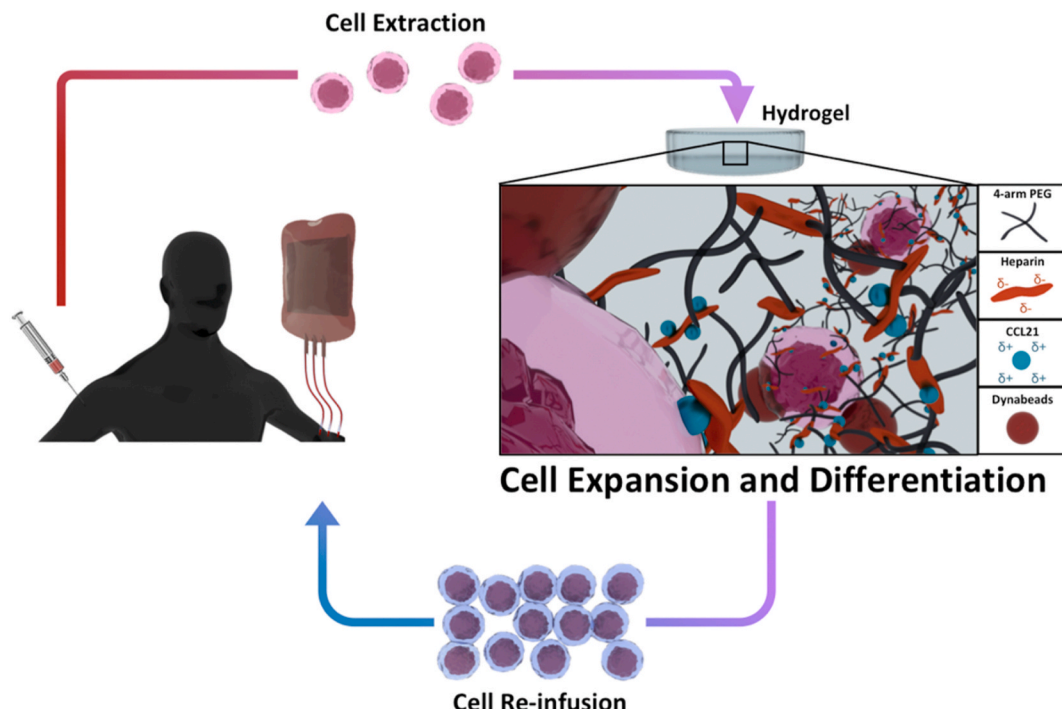


Fig. 1. T cell expansion in a CCL21-loaded PEG-Hep hydrogel as part of an ACT process. Simplified scheme of an ACT process (e.g. without including the genetic modification of the cells or the selection of TILs) with T cells cultured in the CCL21-loaded PEG-Hep hydrogels (not to scale). In our protocol, human primary CD4 $^{+}$ T cells from adult healthy donors were activated with the artificial APCs Dynabeads and used as a proof-of-concept prior to testing with patients. Thus, the expanded T cells were not reinfused.

hydrogels whose chemical stimuli are conveyed through the heparin loading. Additionally, a full characterization of the structural, mechanical, and chemical properties of the PEG-Hep hydrogels is included, which is focused on identifying and obtaining the most suitable hydrogels to mimic the LNs.

2.1.1. Synthesis of Mal-LMWH and PEG-Hep hydrogel formation

A Michael-type reaction was used to functionalize LMWH with a maleimide group yielding a Mal-LMWH derivative (Fig. S1) [48]. The process was left overnight and the final product was purified by dialysis. The success of the reaction was assessed by proton nuclear magnetic resonance (^1H NMR) through the carbon double bond maleimide peak at

6.83 ppm, as well as attenuated total reflection (ATR) spectroscopy with the two bands at 1709 and 1564 cm^{-1} associated to the carbonyl groups and the carbon double bond of the maleimide ring, respectively (Fig. S2). PEG-Hep hydrogels were formed through a maleimide-thiol reaction between the Mal-LMWH derivative and a 4-arm thiolated PEG (PEG-SH) in phosphate buffered saline (PBS), resulting in a covalent crosslink and the consequent gelation (Fig. 2A). Conversely, mixtures of non-functionalized LMWH and PEG-SH did not result in hydrogel formation (Fig. S3).

Hydrogels with different weight percentages of PEG (6%wt, 4%wt, and 3%wt) were formed, while using the same ratio of PEG-SH and Mal-LMWH (1:1.5). The gelation process and mechanical properties of these

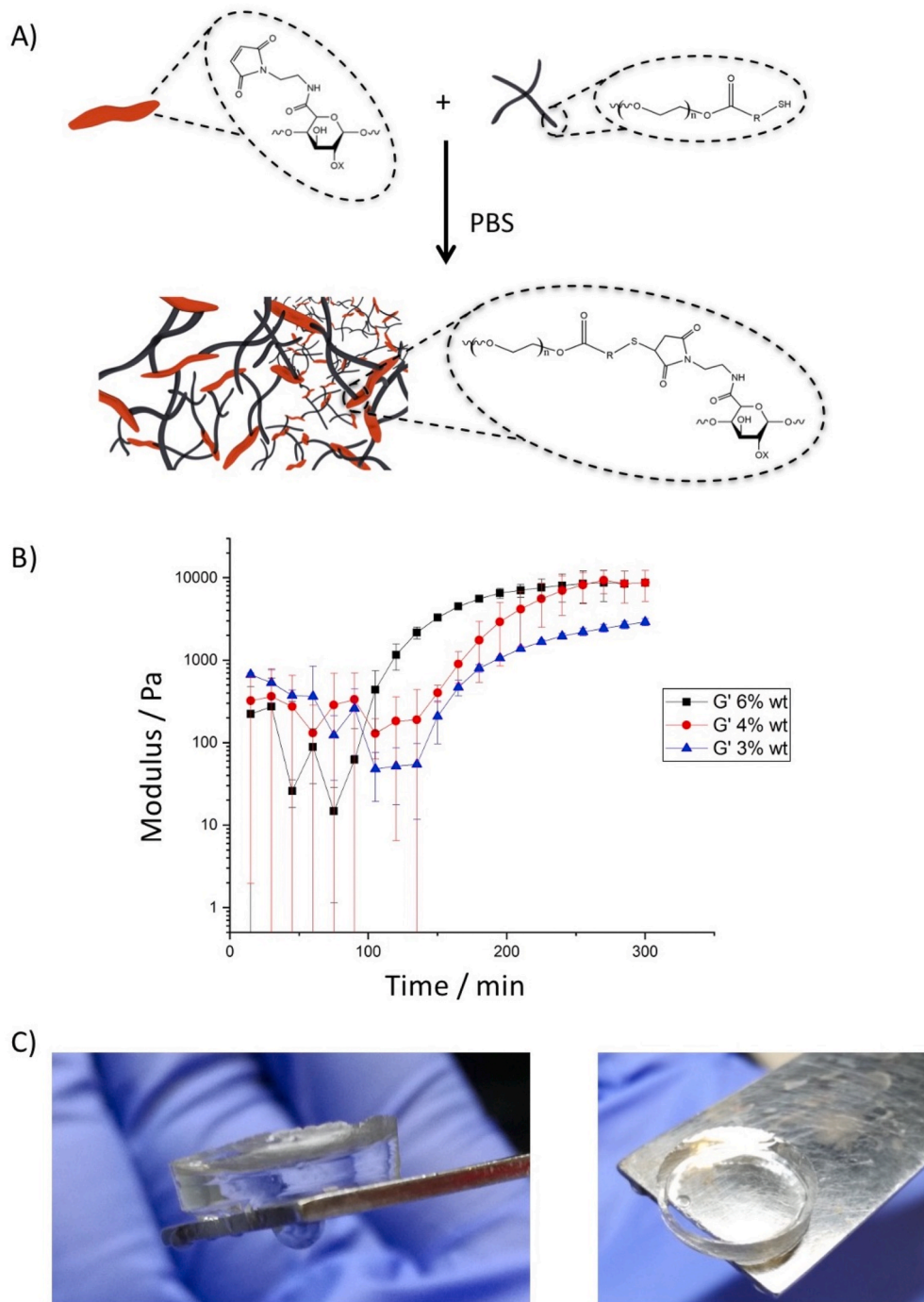


Fig. 2. PEG-Hep hydrogel formation. A) Scheme of the PEG-Hep hydrogel formation, B) time sweeps of 6%wt, 4%wt, and 3%wt PEG-Hep hydrogels and C) lateral-(left) and top-view (right) images of a 6%wt PEG-Hep hydrogel.

hydrogels were characterized by small-amplitude oscillatory shear (SAOS) rheology. The protocol followed was a cycle of sweeps, i.e. time sweep, strain sweep, and frequency sweep, followed by a second time sweep [50]. The final time sweeps were performed at 50 Pa and 0.1 Hz with the rheometer at 37°C (Fig. 2B). The 6%wt PEG-Hep hydrogels were stabilized after ca. 200 min, while the 3%wt PEG-Hep hydrogels required 240 min. All hydrogels were stable for over 48 h in the incubator with cell culture medium (Fig. 2C).

2.1.2. Structural properties of PEG-Hep hydrogels

The three different types of PEG-Hep hydrogels were studied by scanning electron microscopy (SEM) and their pore size ranges were calculated (Fig. 3A).

The median pore size of the 6%wt PEG-Hep hydrogels is 20 µm with a porosity range of 5–50 µm, which increases to 40 µm for the 4%wt hydrogels with a range of 20–75 µm, and to 55 µm with a range of 25–105 µm for the 3%wt PEG-Hep hydrogels. Thus, the lower the amount of PEG, the higher the porosity of the hydrogel, as expected. Pore sizes of 80 µm were described to result in unconstrained migration, similar to the one observed in collagen, the major ECM protein of the LNs, unlike smaller pore sizes (20–40 µm) [51]. We hypothesize that the median pore size of ca. 55 µm that we obtained might be even more adequate than larger pore sizes for T cell activation, as it might introduce minimal constraints to ensure the formation of the immunological synapse between T cells and the artificial APCs Dynabeads, which has

been described to occur in periods of time ranging from a few minutes up to 2 days for CD4⁺ T cells [52–54]. Moreover, it is known that T cells aggregate together with Dynabeads when they proliferate resulting in clusters [12,55,56]. Thus, the 3%wt hydrogels are also more suitable than the 4%wt and 6%wt ones to allow such aggregates. Additionally, 3%wt PEG-Hep hydrogels were freeze-dried and their 3D structure was characterized by X-ray microtomography. Thus, the internal structure of the hydrogels could be observed, revealing pore interconnectivity, in agreement with the SEM images (Fig. 3B). Although we cannot entirely discard an increase in interconnectivity caused by the effect of the freeze-drying process, primary human CD4⁺ T cell infiltration in 3%wt PEG-Hep hydrogels was demonstrated by confocal microscopy over large areas, using hydrogels that were not submitted to such process (Figs. 3C and S4). To visualize the cells inside the hydrogels, they were stained with carboxyfluorescein diacetate succinimidyl ester (CFSE), an intracellular dye that is only fluorescent in viable cells. Finally, the swelling ratio of the 3%wt PEG-Hep hydrogels in PBS was determined to be 18.5 ± 1.2 [57].

2.1.3. Chemical properties: loading capacity of the PEG-Hep hydrogels

PEG-Hep hydrogels are expected to be a well-defined platform whose chemical stimuli are specifically provided by interactions with the negatively charged heparin units, given the inert character of PEG. Indeed, the capacity of heparin (UFH and LMWH) to electrostatically interact with positive binding sites of proteins is the basis for its

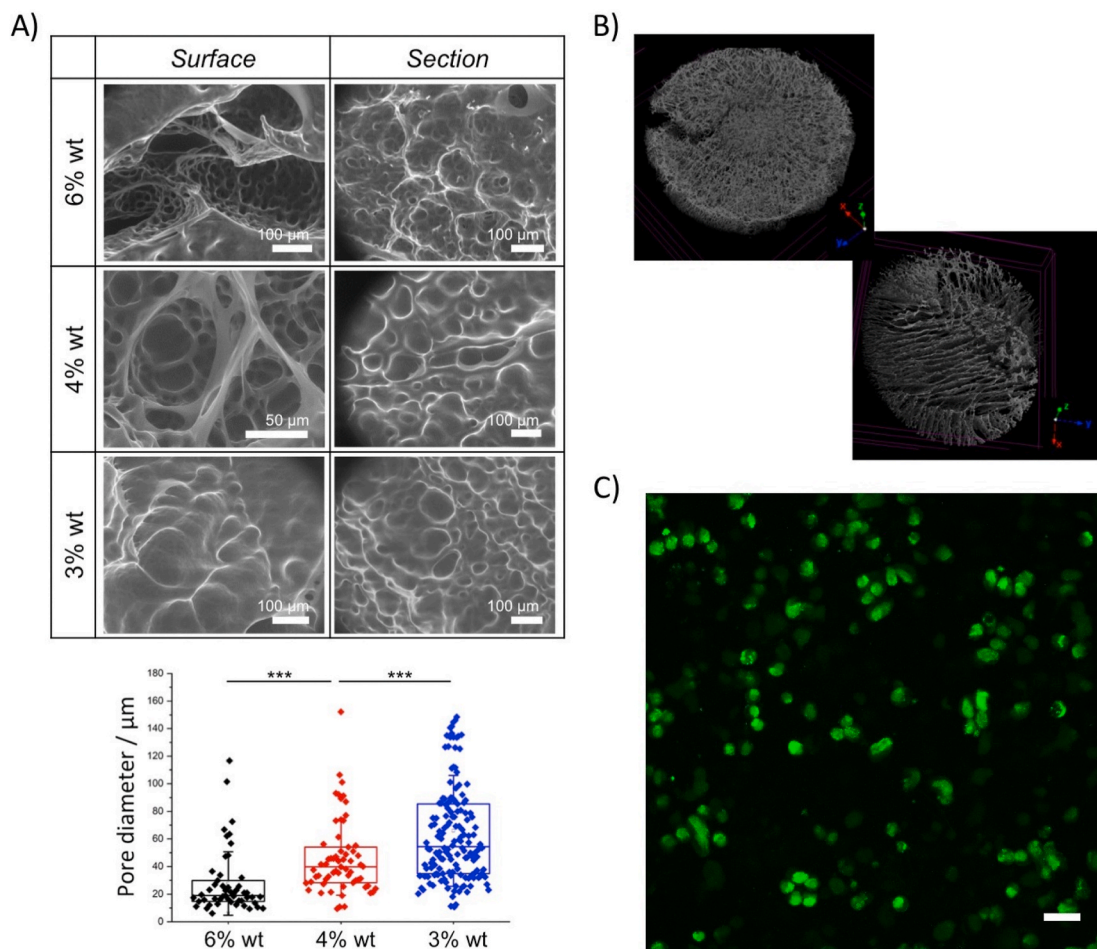


Fig. 3. Structural properties of PEG-Hep hydrogels. A) SEM images and pore size evaluation of PEG-Hep hydrogels with different compositions of PEG (6%wt, 4%wt, and 3%wt). The statistical significance was determined by the Kruskal Wallis ANOVA test (**p < 0.001). B) X-ray microtomographs of a 3%wt PEG-Hep hydrogel of 1 cm of diameter (top-left image) and a small homogeneous zone (3.5 mm of diameter and 500 µm of height) used to analyze its porosity (bottom-right image). C) Confocal maximum projection showing CFSE-stained primary human CD4⁺ T cells in 3%wt PEG-Hep hydrogels after 5 days of incubation (scale bar = 20 µm).

application as anticoagulant and protein stabilizer, as mentioned before [40]. The estimated charge of UFH is approximately -75 , which has been calculated considering that on average, there are 2.7 sulfate groups per disaccharide monomer, the repeating units of heparin consisting of uronic acid and glucosamine in a 1,4-linkage, and heparin has an averaged molecular weight of 15 kDa [40,58,59]. Considering that the LMWH here used is reported to have an averaged molecular weight of 5 kDa according to the provider, an estimated charge of ca. -25 is expected.

To corroborate the electrostatic interaction between LMWH and positively charged units, LMWH was incubated with a model protein

consisting of a modified green fluorescent protein (mGFP), which has an estimated charge of $+5.6$ (see [supplementary data](#)). The resulting mixture was analyzed by dynamic light scattering (DLS) and zeta potential measurements. In the DLS, solutions of LMWH and mGFP showed single peaks at 0.7 ± 0.1 nm and 4.6 ± 0.4 nm, respectively. In contrast, the measurements of the mixture of LMWH and mGFP resulted in a main peak at 5.4 ± 0.4 nm, which is larger than any of the reactants alone, thus suggesting that there is interaction between them ([Fig. 4A](#)). Additionally, there is a broad band around 25 nm in the mGFP that also grows in percentage when the Mal-LMWH is present.

The zeta potential measurements were performed in PBS, which

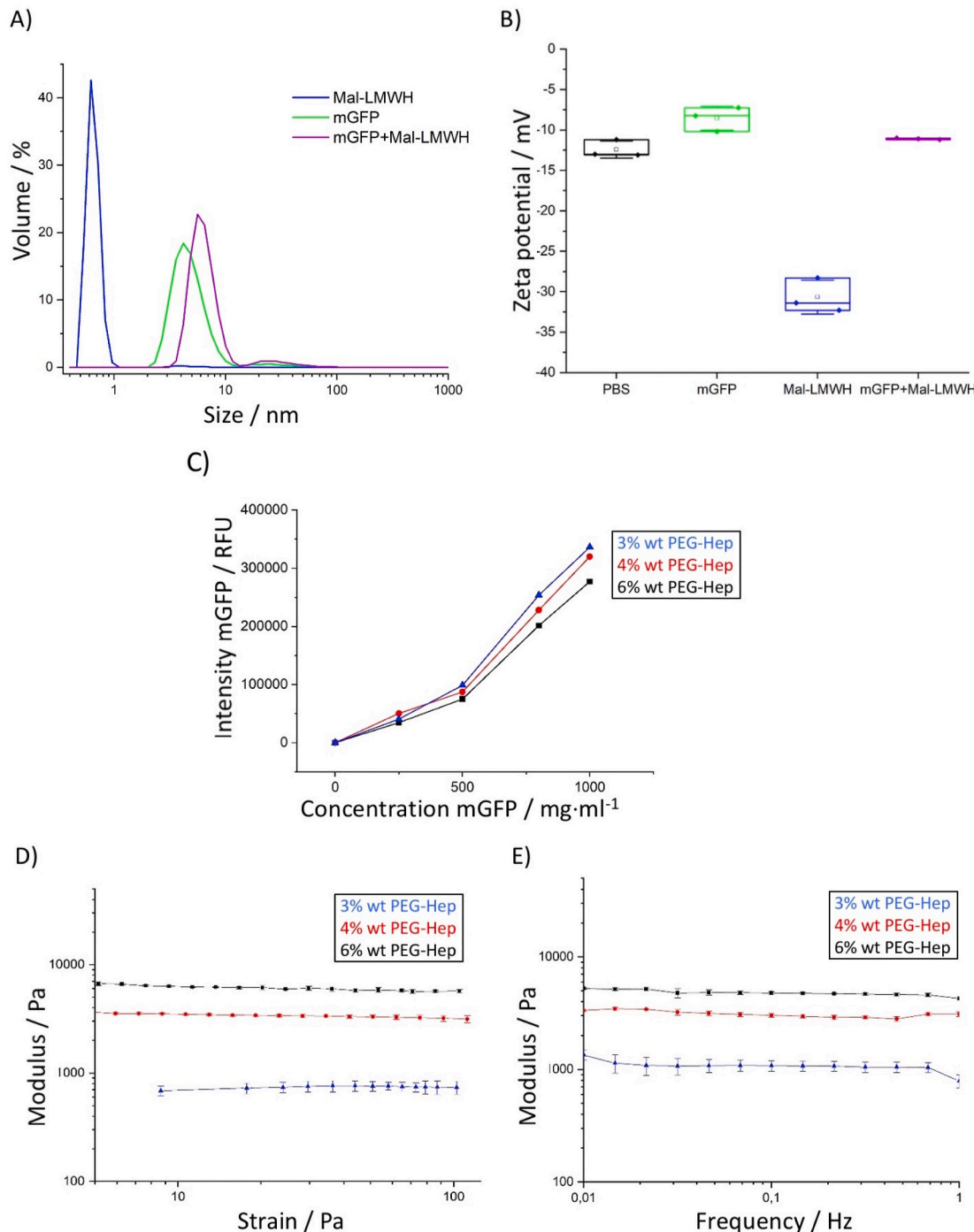


Fig. 4. Chemical and mechanical properties of PEG-Hep hydrogels. A) DLS and B) zeta potential of Mal-LMWH, mGFP, and a mixture of both. C) Loading curve of 6% wt, 4% wt, and 3% wt PEG-Hep hydrogels with mGFP. D) Strain sweeps and E) frequency sweeps of 6% wt, 4% wt, and 3% wt PEG-Hep hydrogels.

showed a value of -13.0 mV. The LMWH and mGFP exhibited values of -31.4 mV and -8.3 mV, respectively, whereas the mixture was almost neutralized with a value of -11.1 mV, similar to PBS (Fig. 4B). Thus, these results support the reported evidence on the capacity of heparin to interact with positively charged units.

Finally, PEG-Hep hydrogels were also incubated with the mGFP during 1 h. After proper rinsing with PBS, the resulting fluorescence of the hydrogels was measured (Fig. 4C). The 3%wt PEG-Hep hydrogel shows a higher retention capacity than the 4%wt and the 6%wt PEG-Hep hydrogels, suggesting that it has a better pore interconnectivity that allows the mGFP solution to easily diffuse into the hydrogel.

2.1.4. Mechanical properties of PEG-Hep hydrogels

Fully formed PEG-Hep hydrogels were characterized by rheometry. Strain sweeps were performed at a constant frequency of 1.0 Hz and the pressure was swept from 1 Pa to 150 Pa on the fully formed gel (Fig. 4D). Then frequency sweeps were performed from 0.01 Hz to 10 Hz at a constant strength of 50 Pa (Fig. 4E).

All hydrogels exhibited linear behavior of dynamic modulus (G') from a strength of 10 Pa–100 Pa. The 3%wt PEG-Hep hydrogels showed a G' lower than those of 4%wt and 6%wt. The frequency sweeps were linear from 0.01 Hz to 1 Hz. Similarly, lower G' values were obtained for the 3%wt than the 4%wt and 6%wt PEG-Hep hydrogels. The values of the equilibrium shear modulus (G_0) achieved were 4.8 ± 0.2 kPa for the 6%wt PEG-Hep hydrogels, 3.1 ± 0.1 kPa in the case of the 4%wt PEG-

Hep hydrogels, and 1.1 ± 0.1 kPa for the 3%wt PEG-Hep hydrogels. Thus, hydrogels with less PEG and heparin are softer than those with higher amounts of material, as expected. However, the values obtained are very similar and all in agreement with the reported LN stiffness, which is around 10 kPa as measured by *in vivo* shear-wave elastography [60–63].

2.2. T cell expansion and differentiation using 3D PEG-Hep hydrogels

After the synthesis and physicochemical characterization of the hydrogels, 3 wt% PEG-Hep hydrogels were chosen to culture T cells given their largest pore size and highest interconnectivity, while keeping adequate mechanical properties. To perform these experiments, primary human CD4⁺ T cells of healthy adult donors were used as a relevant population in the clinics [64–69], but also due to their highest natural occurrence in peripheral blood in comparison to other populations of clinical interest such as CD8⁺ or regulatory T cells. T cell proliferation and differentiation were measured on days 5–6 as a standard proliferation time point that allows to assess the success of the (loaded) 3D structures [55,70]. The effect of immobilizing CCL21 compared to having it in solution on CD4⁺ T cell cultures was first confirmed using planar surfaces to reduce the complexity of the system given by the 3D structure. Additionally, these experiments allowed us to establish an initial concentration range to load the hydrogels.

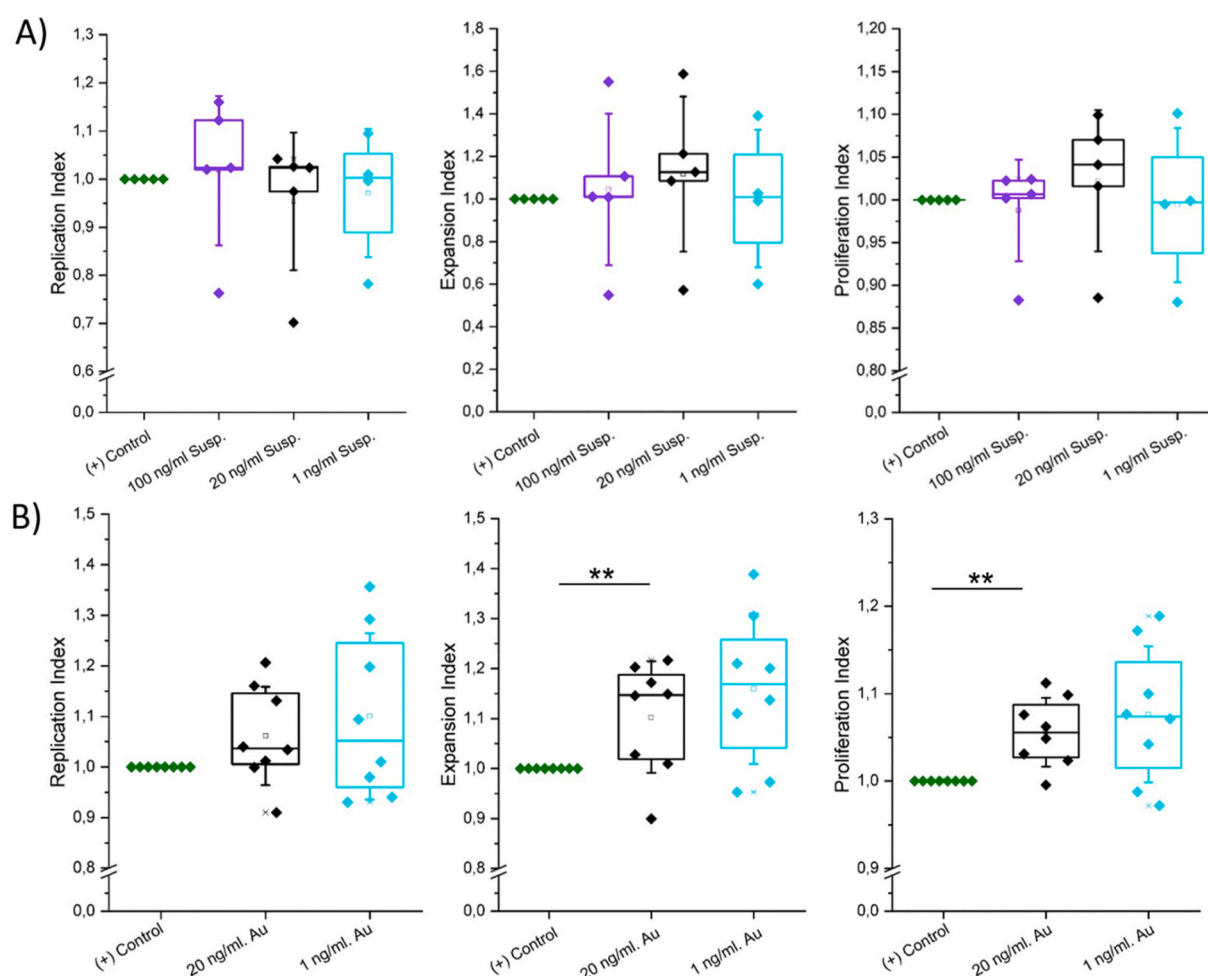


Fig. 5. Effect of CCL21 immobilization on CD4⁺ T cell expansion. Normalized proliferation analysis of CD4⁺ T cells 6 days after seeding with Dynabeads and different concentrations of CCL21 A) in suspension ($N_{\text{donors}} = 5$, with a minimum of $N_{\text{donors}/\text{condition}} = 4$) and B) fixed to Au surfaces ($N_{\text{donors}} = 8$). The replication index (fold-expansion of the responding cells), expansion index (fold-expansion of the overall culture), and proliferation index (average number of divisions among the responding cells) were measured. Statistical significance was determined by the Mann-Whitney U test (** $p < 0.01$).

2.2.1. Effect of CCL21 immobilization on CD4⁺ T cell expansion

CCL21 is a cytokine with an estimated charge of +17.0 that costimulates the expansion of CD4⁺ T cells and is immobilized in the LNs through heparan, as mentioned before. Prior to loading CCL21 to the hydrogel, the effect of its immobilization was studied. With this objective, different concentrations of CCL21 were seeded in suspension and fixed on planar gold (Au) surfaces through its cysteine groups, given the well-known anchoring capacity of Au through the formation of covalent

thiol-Au bonds (Fig. S5) [71]. The concentrations chosen were 1 ng/ml, 20 ng/ml, and 100 ng/ml for experiments in suspension as well as 1 ng/ml and 20 ng/ml for the CCL21-immobilized surfaces (Figs. 5 and S6). Elevated concentrations of CCL21 were avoided given their potentially inhibitory effect [72].

Thus, CD4⁺ T cell proliferation was evaluated by flow cytometry through CFSE stainings. Specifically, the expansion, replication, and proliferation indexes were calculated with the software FlowJo (see

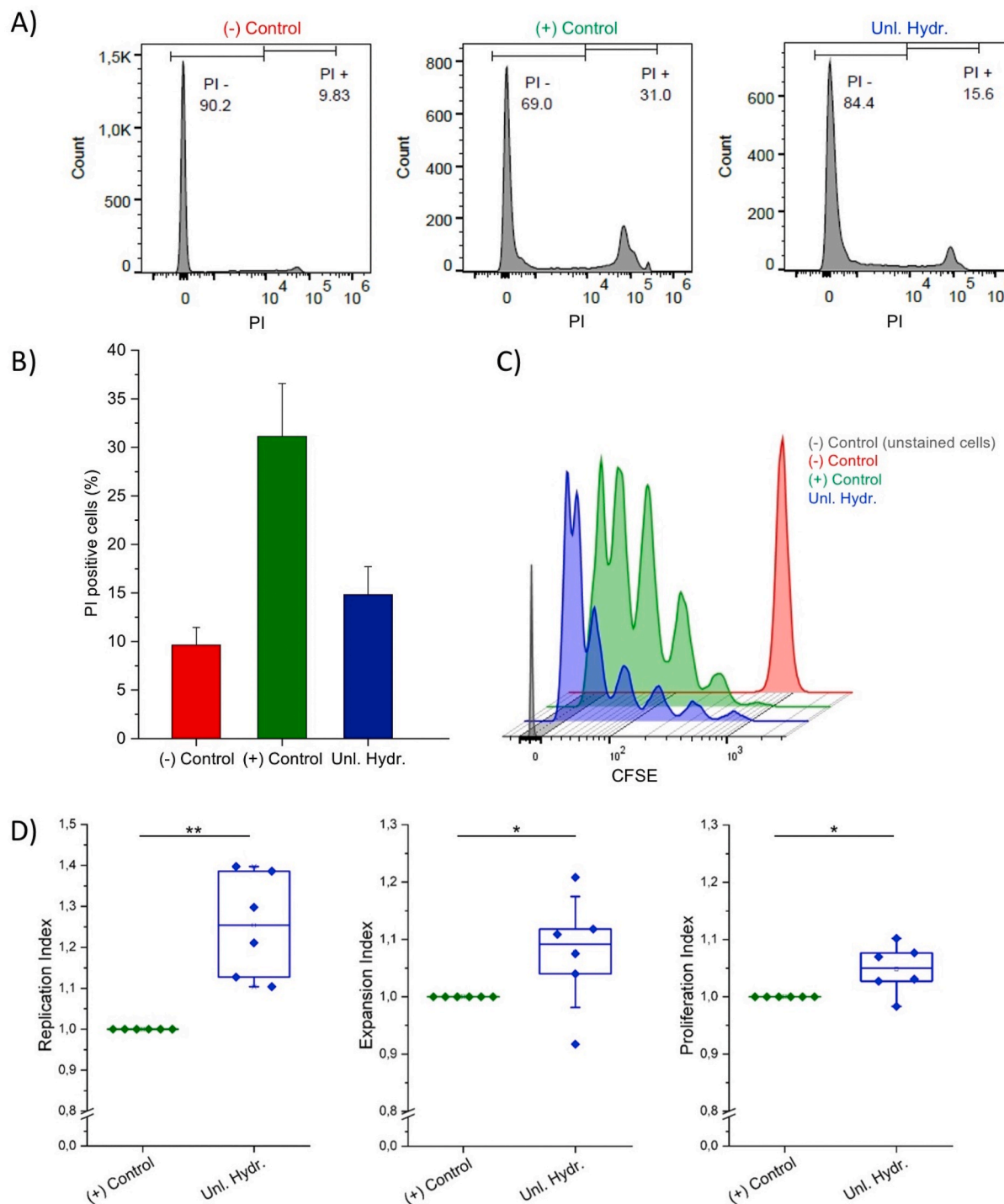


Fig. 6. Effect of 3D PEG-Hep hydrogels on CD4⁺ T cell proliferation. A) Representative flow cytometry histograms of the B) propidium iodide (PI) viability test performed to CD4⁺ T cells seeded on 3 wt% PEG-Hep hydrogels. Bars are mean + standard deviation ($N_{\text{donors}} = 3$). C) Representative CFSE diagram of D) normalized replication, expansion, and proliferation indexes of CD4⁺ T cells stimulated with Dynabeads 5 days after seeding in unloaded 3 wt% PEG-Hep hydrogels ($N_{\text{donors}} = 6$). Statistical significance was determined by the Mann-Whitney U test (*p < 0.05, **p < 0.01).

supplementary data) [73]. The expansion and replication indexes determine the fold-expansion of the overall culture and that of the responding cells, respectively. The proliferation index is the average number of divisions that all responding cells have undergone since the beginning of the culture. These three parameters are therefore relevant for cell therapy, showing how responsive the cells are to the proliferative stimulus and how many cells can be obtained.

To minimize the variability caused by the different donors, the results obtained were normalized relative to the positive controls ($CD4^+$ T cells stimulated in suspension with Dynabeads) of each independent experiment. Thus, the value of all indexes for the positive control is 1. The negative controls correspond to $CD4^+$ T cells seeded in suspension without Dynabead stimulation.

As shown above, no significant differences could be observed among the different CCL21 concentrations in suspension (Figs. 5A and S6A). The median values for the replication index for 100 ng/ml, 20 ng/ml, and 1 ng/ml were 1.01, 0.95, and 0.96, respectively, i.e. very close to the positive controls. The same tendency was observed for the expansion index, with median values of 0.99, 1.02, and 0.99, and the proliferation index with values of 1.05, 1.12, and 1.00 for 100 ng/ml, 20 ng/ml, and 1 ng/ml, respectively. In contrast, immobilizing CCL21 on Au surfaces (Figs. 5B and S6B) resulted in significant changes for the proliferation and expansion indexes. Specifically, the median values for the expansion index were of 1.10 and 1.16 for the concentrations of 20 ng/ml and 1 ng/ml respectively, showing an improvement of 10% and 16% in

comparison with the positive control. Similarly, the proliferation index increased to 1.06 and 1.08 for each concentration. The replication index also showed a slight increase with median values of 1.06 for 20 ng/ml and 1.10 for 1 ng/ml.

2.2.2. Effect of 3D PEG-Hep hydrogels on $CD4^+$ T cell proliferation

As mentioned above, the 3%wt PEG-Hep hydrogels were selected to culture $CD4^+$ T cells activated with Dynabeads, which enabled cell infiltration and thus a truly 3D culture (Figs. 3C and S4). Moreover, a propidium iodide (PI) viability test was performed, which showed more non-viable or apoptotic PI⁺ cells in suspension cultures (positive control; 31%) than when 3%wt hydrogels were used (15%) through flow cytometry (Fig. 6A and B). $CD4^+$ T cell proliferation was then assessed through the expansion, replication, and proliferation indexes obtained from CFSE diagrams (Fig. 6C) also through flow cytometry.

First, unloaded 3%wt PEG-Hep hydrogels were used as a scaffold to study $CD4^+$ T cell proliferation on day 5 (Figs. 6D and S7). The median normalized replication index obtained in these 3%wt PEG-Hep hydrogels was 1.25, i.e. an improvement of a 25% was achieved, whereas the expansion and proliferation indexes showed medians of 1.10 and 1.05, respectively. All three parameters showed statistically significant increases compared to the positive controls. The most significant improvement was observed for the replication index, which indicates that the responding cells that get activated in the synthetic hydrogels proliferate more than the activated cells in suspension.

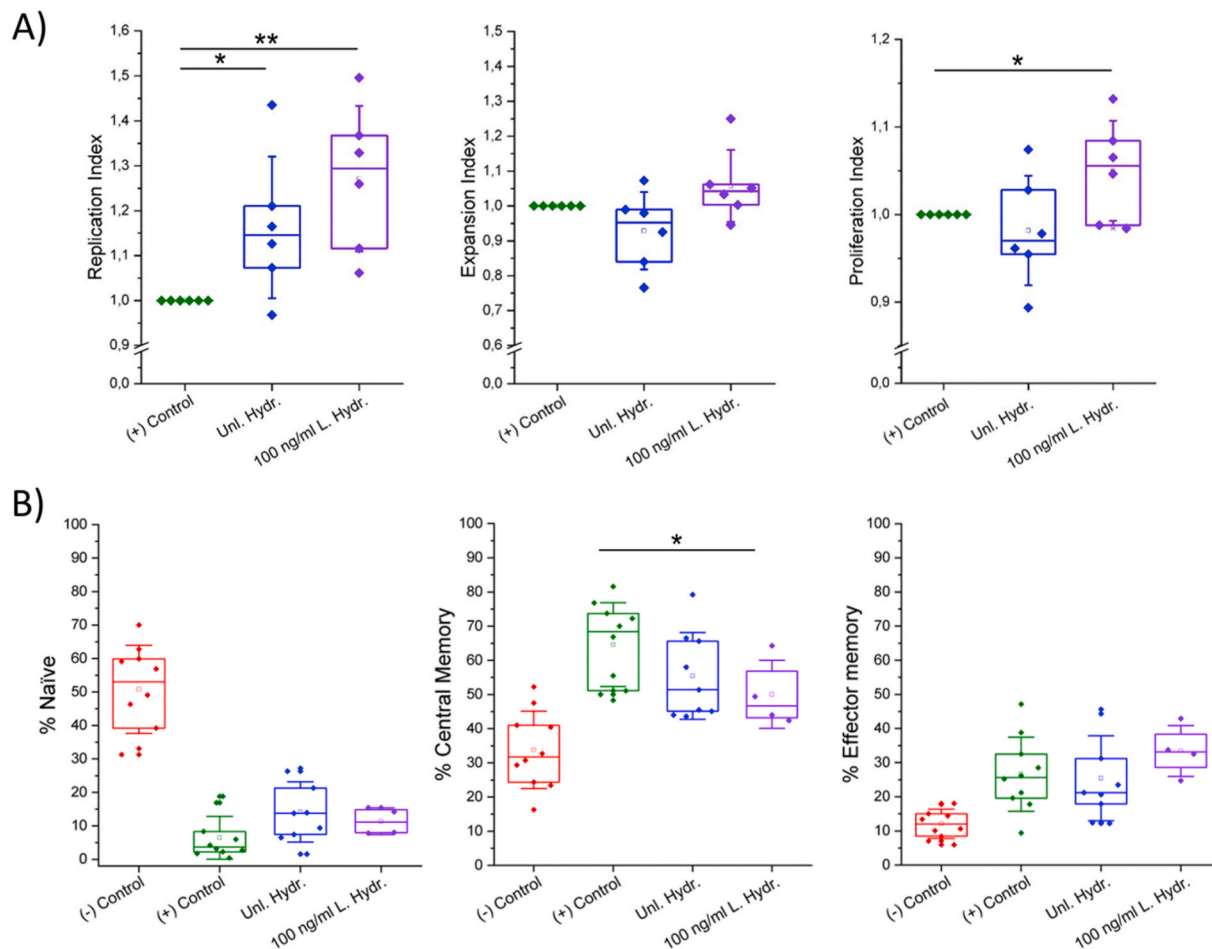


Fig. 7. Effect of CCL21-loaded 3D PEG-Hep hydrogels on $CD4^+$ T cell proliferation and differentiation. A) Normalized proliferation analysis of $CD4^+$ T cells stimulated with Dynabeads 6 days after seeding in 3 wt% PEG-Hep hydrogels loaded with 100 ng/ml of CCL21 ($N_{\text{donors}} = 6$). B) Percentage of naïve (T_N), central memory (T_{CM}), and effector memory (T_{EM}) $CD4^+$ T cells on day 5 ($N_{\text{donors}} = 6$). The negative control consists of cells seeded in suspension without Dynabeads, whereas in the positive control, cells are seeded with Dynabeads. When cells are seeded in the hydrogels, they are always stimulated with Dynabeads. Statistical significance was determined by the Mann-Whitney U test (* $p < 0.05$, ** $p < 0.01$).

2.2.3. Effect of CCL21-loaded 3D PEG-Hep hydrogels on CD4⁺ T cell proliferation and differentiation

Hydrogels were finally loaded with different concentrations of CCL21 and 100 ng/ml was identified as the one resulting in the highest expansion indexes (Figs. S8 and 7A). The difference between this result and the values obtained with the CCL21-immobilized surfaces (Fig. 7B) are, most probably, due to the increased dimensionality when moving from 2D to 3D biomaterials. In this case, a 29% increase of the replication index on day 6 was obtained in comparison with the positive control. The proliferation and expansion indexes showed less pronounced increases with average values of 1.05 and 1.06, respectively. Although not statistically significant, we observed slight decreases in the expansion and replication indexes without cytokine loading, which evidence the importance of the timings when extrapolating the results to the clinics.

To determine the phenotype of the CD4⁺ T cells after proliferation, differentiation assays were performed 5 days after seeding (Figs. 7B and S9), given its importance in the clinical outcomes obtained in ACT [16, 74]. Specifically, naïve (T_N; CD45RO⁻/CD62L⁺), central memory (T_{CM}; CD45RO⁺/CD62L⁺), and effector memory (T_{EM}; CD45RO⁺/CD62L⁻) cells were identified by flow cytometry [67]. The percentages of CD4⁺ T cells that express CD45RO and CD62L prior to stimulation (negative control) are affected by intrinsic donor variability. As expected, they mainly showed a T_N phenotype with a median value of 53%, whereas the T_{EM} and T_{CM} phenotypes were found in smaller percentages, 12% and 32%, respectively. After stimulation, the median value of T_N cells decreased to 4% in suspension (positive control). Both unloaded and loaded (100 ng/ml of CCL21) hydrogels also exhibited a decrease of this phenotype with median values of 14% and 11% respectively, although it is more preserved than in the suspension cells. Consequently, the T_{EM} and T_{CM} phenotypes increased in comparison with the negative control. Specifically, the median values for the T_{CM} phenotype of the positive control, unloaded and loaded hydrogels were 68%, 51%, and 47%, respectively, thus expressing lower percentages when using hydrogels. For the T_{EM} phenotype, median values rose to 26% for T cells in suspension, 21% for unloaded hydrogels, and 33% for hydrogels with 100 ng/ml of CCL21. Thus, the cytokine loaded hydrogels promoted an increased proportion of effector cells. These results point out that PEG-Hep hydrogels can be used to modify the resulting phenotype of T cells and the use of different chemical stimuli is a promising strategy to achieve diverse differentiation pathways.

Thus, the fabrication of an artificial matrix capable of mimicking the ECM of SLOs is expected to be a powerful approach to promote immune cell expansion as well as preserve and augment T cell cytotoxicity towards cancer cells [21,22,51]. The use of these matrices in cellular immunotherapies, which require the removal and culture of T cells *ex vivo* to expand them several thousand-fold, could be useful towards overcoming current limitations [8,75]. The 3D PEG-Hep hydrogels here employed showed an interconnected porous structure with adequate rheological properties to mimic the physical structure of the LNs [61–63, 76], and favor CD4⁺ T cell migration through the matrix [51]. Moreover, the capacity of the hydrogels to retain positively charged molecules has been shown, opening the way to introduce other biomolecules, such as adhesion molecules (e.g. ICAM-1), which could improve the mimicking and understanding of the ECM of the LNs and its interaction with cells [56,77,78]. These tunable characteristics should provide advantages compared to the current commercial platforms, such as 3D polystyrene scaffolds and Matrigel, which showed intrinsic limitations as they were not designed for this purpose [20]. Additionally, the hydrogels here proposed are an excellent system to distinguish the effects of the LNs from the APCs, which we mimicked with Dynabeads. In contrast, a recently reported interesting system based on PEG hydrogels combined with hyaluronic acid to mimic the lymphoid tissue was functionalized with antiCD3 and antiCD28, thus also providing APC signals [79]. Moreover, our hydrogels contain heparin, as a derivate of the heparan sulfate groups that cover the lymphoid tissues and serve as

anchoring for relevant molecules [23,24]. Nevertheless, the unloaded hydrogels already resulted in an improvement of CD4⁺ T cell proliferation and changes in the resulting phenotypes, demonstrating the benefits of the physical characteristics of the 3D PEG-Hep scaffolds. The addition of CCL21, which showed better results immobilized than in suspension, enhanced CD4⁺ T cell proliferation and accentuated the differences in the phenotypes. These results show the potential that 3D PEG-Hep hydrogels hold as a platform for T cell culture, which could be further improved by adding other chemical molecules, such as CCL19 and ICAM-1, to maximize successful clinical outcomes [80–83]. Moreover, the characteristics of these hydrogels make them suitable for complementary applications such 3D (bio)printing or *in vivo* local delivery of pre-activated T cells, similar to other materials [84]. All these options will be evaluated in the future along with *in vitro* experiments not only with CD4⁺ T cells, but also with other medically relevant phenotypes such as CD8⁺ and regulatory T cells.

3. Conclusions

In conclusion, CCL21-loaded 3D PEG-Hep hydrogels were synthesized, characterized, and used for CD4⁺ T cell culturing. This scaffold provides an improvement in cell proliferation and an influence on the phenotype, which could be further explored towards the fabrication of artificial LNs. These engineered organs are expected to help surpassing the limitations of current immunotherapies such as producing large amounts of T cells with therapeutic phenotypes. Moreover, the CCL21-loaded 3D PEG-Hep hydrogels are expected to be compatible with perfusion systems and novel bioreactors to work under good manufacturing practice (GMP) conditions in large facilities.

4. Materials and methods

Materials: The mGFP was produced and purified as described elsewhere [85]. LMWH was purchased from Fisher Scientific (Fisher Bio-Reagents, Spain). The CD4⁺ T cell isolation kit was acquired from Miltenyi Biotec GmbH (Germany). NuncTM Lab-TekTM chambers, fetal bovine serum (FBS), penicillin/streptomycin (P/S), CellTrace CFSE cell proliferation kit, and Dynabeads were provided by Thermo Fisher Scientific (USA). The anti-human CD3 FITC, CD4 PE, CD45RO FITC antibodies and their controls used for flow cytometry were acquired from Immunotools GmbH (Germany), whereas CD62L PE and its control were bought from BioLegend (USA). Lymphoprep was obtained from Stemcell Technologies (Canada). PEG-SH (Mn 10,000 g/mol), *N*-(2-aminoethyl) maleimide trifluoroacetate salt (AEM), 1-hydroxybenzotriazole hydrate (HOBT), *N*-(3-dimethylamino-propyl)-*N'*-ethylcarbodiimide hydrochloride (EDC·HCl), 2-(*N*-morpholino) ethanesulfonic acid (MES), exodus-2 (CCL21) human, Dulbecco's PBS, RPMI-1640 media, and the rest of the products not otherwise specified were purchased from Sigma-Aldrich (USA).

Synthesis and optimization of LMWH functionalized with maleimide: The functionalization of LMWH with maleimide was based in a method previously described [86,87]. For 100 mg of LMWH dissolved in a solution of 0.1 M MES, 20.6 mg of HOBT, 20.6 mg of AEM, and 20.6 mg of EDC·HCl were used (Fig. S1). To maximize the yield, the reaction was left overnight. The product was purified by dialysis (MWCO 1000) against 500 ml of deionized water for 6–15 h during the first step, and 500 ml of MilliQ water during the second and last steps. Once the product was purified, it was lyophilized and characterized by ¹H NMR and ATR (Fig. S2). ¹H NMR (250 MHz, H₂O-*d*₂, δ): 6.83 ppm (s, 2H, CH=CH); ATR: ν = 1709 (C=O), 1564 (CH=CH) cm⁻¹.

PEG-Hep hydrogel formation: A solution of PEG-SH was mixed with a solution of the functionalized Mal-LMWH in a 1:1.5 ratio, both in PBS. For such ratio, five maleimide groups per molecule of heparin were estimated to react with the four thiol groups of PEG [87]. Different concentrations in weight of PEG were used (6%wt, 4%wt, and 3%wt) to obtain different types of PEG-Hep hydrogels. Once the solutions were

mixed, they were kept in an incubator at 37°C during at least 2 h to become a hydrogel. Negative controls consisting of solutions of only one of the reactants as well as a mixture of non-functionalized LMWH and PEG-SH at relevant concentrations confirmed that hydrogel formation is caused by the reaction between the thiol groups of the 4-arm PEG and the maleimide-functionalized LMWH (Fig. S3).

Swelling ratio: The swelling ratio of the 3%wt PEG-Hep hydrogels was determined in PBS using the formula W_s/W_d , where W_s and W_d are the weight of the swollen and dry hydrogel, respectively ($N_{samples} = 3$).

Scanning electron microscopy (SEM): Although this technique is typically used in dry samples, a special protocol at the vacuum chamber was used, which enabled to image the structure of the hydrated hydrogels. Thus, the structure of hydrogels with different compositions (6%wt, 4% wt, and 3%wt of PEG) was observed. The equipment used was a FEI Quanta 650F Environmental scanning electron microscope (Thermo Fisher Scientific, USA).

X-ray microtomography: A Skyscan 1272 high-resolution micro computed tomography (Bruker, USA) was used to study the 3D structure of the hydrogels and analyze the porosity and interconnectivity of the pores. Samples stored in PBS were frozen with liquid nitrogen and then lyophilized to be scanned. The size of the measured samples was 2 mm in height and 1 cm in diameter. The scanning time was 3 h with a minimum resolution of 5 μm.

Confocal microscopy: The images were obtained with a Leica TCS SP5 confocal microscope (Leica, Germany) equipped with 10X and 63X objectives on day 5.

Dynamic Light Scattering (DLS) and zeta potential: Solutions of LMWH (8.9 μM), mGFP (27.0 μM), and a mixture of mGFP (27.0 μM) with 0.045 mg of LMWH, were prepared in PBS. The solution of PBS was also measured as a control. All samples were passed through a filter (0.22 μm) and vortexed before measurements. 1 ml of each resulting suspension was measured at least three times with three single runs per measurement at 25°C using a Zetasizer Nano ZS (Malvern Panalytical Ltd, UK).

Loading capacity of the hydrogels: To demonstrate the ability of PEG-Hep hydrogels to attract positively charged molecules to their negatively charged LMWH, different concentrations of mGFP were incubated with the hydrogels during 1 h. After that, the supernatant was removed and the hydrogels were washed three times with PBS. The fluorescence of the hydrogels was measured with a Victor 3 Multioption plate reader (Perkin Elmer, Inc., USA).

Rheology measurements: The SAOS technique was used to characterize the mechanical properties of the hydrogels. It consists of a small-amplitude torsional oscillation that generates a shear flow in the sample and requires a trial-and-error approach to find the appropriate values of strain and frequency for each gel [50]. The experiments performed were strain sweeps, frequency sweeps, and time sweeps at 37°C to calibrate the range of pressure and frequency where the hydrogels maintain their viscoelastic behavior, characterize the gelification processes, and obtain the G_e value of the gels. Thus, the G' and loss modulus (G'') in the linear-viscoelastic regime (LVE) of the hydrogels were measured. The equipment used was a Rheometer HAAKE RheoStress RS600 (Thermo Electron Corporation, USA) with a 10 mm diameter rotor.

Preparation of Au surfaces to immobilize CCL21: The function of CCL21 and its effect on T cell proliferation was studied in suspension and immobilized on Au surfaces to analyze the influence of fixing this cytokine on CD4⁺ T cell proliferation. To prepare the Au samples, glass slides were thoroughly washed with piranha solution and coated with 3 nm of titanium and 10 nm of Au in an evaporation System Auto 306 (Boc Edwards, UK). The resulting Au surfaces were fixed to the bottom of 8-well Lab-Tek chambers with picodent twinsil speed glue (Picodent, Germany). Then, CCL21 was incubated during 1 h at the desired concentration and the supernatant was subsequently removed. Finally, cells were seeded on the substrates. To prove the success of the surface functionalization strategy, an immunostaining was performed (Fig. S5).

CD4⁺ T cell culture in PEG-Hep hydrogels: Primary human CD4⁺T cells of healthy adult donors were obtained from buffy coats provided by “Banc de Sang i Teixits” (Barcelona, Spain) after the approval of the research project by the “Ethics Committee on Animal and Human Experimentation” of the Autonomous University of Barcelona (Nr. 3511) following an established protocol [11,12]. Briefly, it consists of isolating peripheral blood mononuclear cells (PBMCs) by density gradient centrifugation using Ficoll and then extracting the CD4⁺ T cells with a commercial CD4⁺ T cell isolation kit. The purity of the cells was measured by flow cytometry with the antibodies anti-human CD3 FITC, anti-human CD4 PE, and the negative controls. Only samples that were at least 90% positive for both CD3⁺ and CD4⁺ (usually CD3⁺CD4⁺ T cells > 95%) were used. Afterwards the cells were kept in RPMI medium with 10% FBS and 1% P/S in the incubator at 37°C overnight. Similarly, 3%wt PEG-Hep hydrogels were also incubated overnight in PBS to achieve complete swelling. On the next day, the resulting hydrogels were placed in 96-well plates and CD4⁺ T cells (10⁶ cells/ml) and Dynabeads (1:1 ratio) in the supplemented RPMI medium were seeded on them, given that the pore size and interconnectivity of the hydrogels ensures their proper infiltration through the structure. For the CCL21-loaded hydrogels, 100 μl of the chosen CCL21 solution were incubated during 1 h, after which the supernatant was removed, prior to cell seeding.

Propidium iodide (PI) viability test: CD4⁺ T cells were stained with 0.5 μl of propidium iodide (1 mg/ml, Sigma-Aldrich) during 3 min at room temperature before the flow cytometry measurements.

CD4⁺ T cell proliferation and differentiation in PEG-Hep hydrogels: CD4⁺ T cells used for proliferation analysis were stained before seeding with a CFSE cell proliferation kit following the instructions of the manufacturer. They were analyzed by flow cytometry on day 6 after mechanically destroying the hydrogels through pipetting to recover the cells. The results obtained were normalized to the positive control of each donor, which was assigned a value of 1, to reduce the intrinsic donor variability. Raw data can be seen in the supplementary data (Figs. S6 and S7). For the differentiation analysis, CD4⁺ T cells were extracted from the hydrogels as described above and analyzed 5 days after seeding. Cells were stained with anti-human CD45 RO FITC, CD62L PE, and the corresponding negative controls for 30 min at 0°C. Afterwards, they were washed and analyzed by flow cytometry with a BD FACSCanto (BD Bioscience, USA).

Data treatment: The microscope images were treated with Fiji (ImageJ, USA), the flow cytometry data was analyzed with FlowJo (FlowJo LLC, USA), the graphs and statistical tests were performed in Origin (OriginLab Corporation, USA). The boxes of the box plots correspond to the interquartile range defined by the 25th and 75th percentiles, the central line is the median, the whiskers show one standard deviation, – represents the maximum and minimum, and □ is the average.

CRediT authorship contribution statement

Eduardo Pérez del Río: Investigation, Validation, Formal analysis, Writing - original draft, Visualization. **Fabião Santos:** Investigation, Validation, Formal analysis, Visualization. **Xavier Rodríguez Rodríguez:** Investigation. **Marc Martínez-Miguel:** Investigation. **Ramon Roca-Pinilla:** Investigation. **Anna Arís:** Writing - review & editing, Supervision, Funding acquisition. **Elena García-Fruitós:** Writing - review & editing, Supervision, Funding acquisition. **Jaume Veciana:** Writing - review & editing, Supervision, Funding acquisition. **Joachim P. Spatz:** Writing - review & editing, Supervision, Funding acquisition. **Imma Ratera:** Writing - review & editing, Supervision, Project administration, Funding acquisition. **Judith Guasch:** Conceptualization, Methodology, Validation, Writing - original draft, Writing - review & editing, Supervision, Project administration, Funding acquisition.

Declaration of competing interest

The authors declare that they have no known competing financial interests or personal relationships that could have appeared to influence the work reported in this paper.

Acknowledgement

We acknowledge D. P. Rosenblatt for proofreading this manuscript and the “Servei de Microscòpia” from UAB for assistance in the confocal microscopy. The authors are grateful for the financial support received from the Spanish Ministry of Economy and Competitiveness MINECO (MAT2016-80826-R, PID2019-105622RBI00, the “Ramón y Cajal” program (RYC-2017-22614), and a DOC-INIA fellowship), the Networking Research Center on Bioengineering, Biomaterials, and Nanomedicine (CIBER-BBN) through the projects “Alycia” (Nr. BBN18PI01) and “Gels4ACT” (Nr. BBN20PIV02), Generalitat de Catalunya (SGR-918, SGR-229, CERCA Programme, and AGAUR for a pre-doctoral fellowship (FI-AGAUR)), Fundació Marató de TV3 (Nr. 201812), and the European Social Fund. This research was also supported by the People Programme (Marie Curie Actions) of the 7th Framework Programme of the European Union (FP7/2007–2013) through the grant agreement Nr. 600388 of REA with the Agency for Business Competitiveness ACCIÓ through a Tecnicospring fellowship (TECSPR15-1-0015) and the European Union’s Horizon 2020 research and innovation programme H2020-MSCA-COFUND-2016 (DOC-FAM, grant agreement Nr. 754397). The work was funded as well by the Max Planck Society through the Max Planck Partner Group “Dynamic Biomimetics for Cancer Immunotherapy” in collaboration with the Max Planck for Medical Research (Heidelberg, Germany). ICMAB-CSIC acknowledges support from the MINECO through the Severo Ochoa Programme for Centres of Excellence in R&D (SEV-2015-0496; FIP fellowship). This work has been developed inside the biochemistry and biomedicine PhD program of UAB.

Appendix B. Supplementary data

Supplementary data to this article can be found online at <https://doi.org/10.1016/j.biomaterials.2020.120313>.

Data statement

The manuscript included required protocols in detail and data for reproducibility.

References

- [1] K. Servick, War of nerves, *Science* 365 (2019) 1071–1073, <https://doi.org/10.1126/science.365.6458.1071>.
- [2] A.D. Fesnak, C.H. June, B.L. Levine, Engineered T cells: the promise and challenges of cancer immunotherapy, *Nat. Rev. Canc.* 16 (2016) 566–581, <https://doi.org/10.1038/nrc.2016.97>.
- [3] D.L. Porter, W.-T. Hwang, N.V. Frey, S.F. Lacey, P.A. Shaw, A.W. Loren, A. Bagg, K. T. Marcucci, A. Shen, V. Gonzalez, D. Ambrose, S.A. Grupp, A. Chew, Z. Zheng, M. C. Milone, B.L. Levine, J.J. Melenhorst, C.H. June, Chimeric antigen receptor T cells persist and induce sustained remissions in relapsed refractory chronic lymphocytic leukemia, *Sci. Transl. Med.* 7 (2015), <https://doi.org/10.1126/scitranslmed.aac5415>, 303ra139.
- [4] H.M. Zarour, S. Ferrone, Cancer immunotherapy: progress and challenges in the clinical setting, *Eur. J. Immunol.* 41 (2011) 1510–1515, <https://doi.org/10.1002/eji.2011190035>.
- [5] W.A. Lim, C.H. June, The principles of engineering immune cells to treat cancer, *Cell* 168 (2017) 724–740, <https://doi.org/10.1016/j.cell.2017.01.016>.
- [6] S.S. Chandran, R.P.T. Somerville, J.C. Yang, R.M. Sherry, C.A. Klebanoff, S.L. Goff, J.R. Wunderlich, D.N. Danforth, D. Zlott, B.C. Paria, A.C. Sabesan, A.K. Srivastava, L. Xi, T.H. Pham, M. Raffeld, D.E. White, M.A. Toomey, S.A. Rosenberg, U. S. Kammula, Treatment of metastatic uveal melanoma with adoptive transfer of tumor infiltrating lymphocytes: a single-center phase 2 study, *Lancet Oncol.* 18 (2017) 792–802, [https://doi.org/10.1016/S1470-2045\(17\)30251-30256](https://doi.org/10.1016/S1470-2045(17)30251-30256).
- [7] M.E. Dudley, J.R. Wunderlich, T.E. Shelton, J. Even, S.A. Rosenberg, Generation of tumor-infiltrating lymphocyte cultures for use in adoptive transfer therapy for melanoma patients, *J. Immunother.* 26 (2003) 332–342, <https://doi.org/10.1097/00002371-200307000-00005>.
- [8] J.N. Blattman, R. Antia, D.J.D. Sourdice, X. Wang, S.M. Kaech, K. Murali-Krishna, J.D. Altman, R. Ahmed, Estimating the precursor frequency of naïve antigen-specific CD8 T cells, *J. Exp. Med.* 195 (2002) 657–664, <https://doi.org/10.1084/jem.20001021>.
- [9] M.O. Butler, N. Hirano, Human cell-based artificial antigen-presenting cells for cancer immunotherapy, *Immunol. Rev.* 257 (2014) 191–209, <https://doi.org/10.1111/imr.12129>.
- [10] D. Delcassian, S. Sattler, I.E. Dunlop, T cell immunoengineering with advanced biomaterials, *Integr. Biol.* 9 (2017) 211–222, <https://doi.org/10.1039/c6ib00233a>.
- [11] J. Guasch, M. Hoffmann, J. Diemer, H. Riahinezhad, S. Neubauer, H. Kessler, J. P. Spatz, Combining adhesive nanostructured surfaces and costimulatory signals to increase T cell activation, *Nano Lett.* 18 (2018) 5899–5904, <https://doi.org/10.1021/acs.nanolett.8b02588>.
- [12] J. Guasch, C.A. Muth, J. Diemer, H. Riahinezhad, J.P. Spatz, Integrin-assisted T-cell activation on nanostructured hydrogels, *Nano Lett.* 17 (2017) 6110–6116, <https://doi.org/10.1021/acs.nanolett.7b02636>.
- [13] J. Matic, J. Deeg, A. Scheffold, I. Goldstein, J.P. Spatz, Fine tuning and efficient T cell activation with stimulatory AC3 nanoarrays, *Nano Lett.* 13 (2013) 5090–5097, <https://doi.org/10.1021/nl4022623>.
- [14] J. Deeg, M. Axmann, J. Matic, A. Liapis, D. Depoil, J. Afrose, S. Curado, M. L. Dustin, J.P. Spatz, T cell activation is determined by the number of presented antigens, *Nano Lett.* 13 (2013) 5619–5626, <https://doi.org/10.1021/nl403266t>.
- [15] D. Delcassian, D. Depoil, D. Rudnicka, M. Liu, D.M. Davis, M.L. Dustin, I.E. Dunlop, Nanoscale ligand spacing influences receptor triggering in T cells and NK cells, *Nano Lett.* 2013 (2013) 5608–5614, <https://doi.org/10.1021/nl403252x>.
- [16] Y. Li, R.J. Kurlander, Comparison of anti-CD3 and anti-CD28-coated beads with soluble anti-CD3 for expanding human T cells: differing impact on CD8 T cell phenotype and responsiveness to restimulation, *J. Transl. Med.* 8 (2010) 104, <https://doi.org/10.1186/1479-5876-8-104>.
- [17] N.K. Garlie, A.V. LeFever, R.E. Siebenlist, B.L. Levine, C.H. June, L.G. Lum, T cells coactivated with immobilized anti-CD3 and anti-CD28 as potential immunotherapy for cancer, *J. Immunother.* 22 (1999) 336–345, <https://doi.org/10.1097/00002371-199907000-00007>.
- [18] B.L. Levine, W.B. Bernstein, M. Connors, N. Craighead, T. Lindsten, C.B. Thompson, C.H. June, Effects of CD28 costimulation on long-term proliferation of CD4+ T cells in the absence of exogenous feeder cells, *J. Immunol.* 159 (1997) 5921–5930, <https://www.ncbi.nlm.nih.gov/pubmed/9550389>.
- [19] C.H. June, J.A. Ledbetter, P.S. Linsley, C.B. Thompson, Role of the CD28 receptor in T-cell activation, *Immunol. Today* 11 (1990) 211–216, <https://doi.org/10.1146/annurev.yi.11.040193.001203>.
- [20] E. Pérez del Río, M. Martínez Miguel, J. Veciana, I. Guasch, Artificial 3D culture systems for T cell expansion, *ACS Omega* 3 (2018) 5273–5280, <https://doi.org/10.1021/acsomega.8b00521>.
- [21] J.E. Gretz, A.O. Anderson, S. Shaw, Cords, channels, corridors and conduits: critical architectural elements facilitating cell interactions in the lymph node cortex, *Immunol. Rev.* 156 (1997) 11–24, <https://doi.org/10.1111/j.1600-065X.1997.tb00955.x>.
- [22] T. Katakai, T. Hara, J.-H. Lee, H. Gonda, M. Sugai, A. Shimizu, A novel reticular stromal structure in lymph node cortex: an immuno-platform for interactions among dendritic cells, T cells and B cells, *Int. Immunol.* 16 (2004) 1133–1142, <https://doi.org/10.1093/intimm/dxh113>.
- [23] K. Uchimura, M. Morimoto-Tomita, A. Bistrup, J. Li, M. Lyon, J. Gallagher, Z. Werb, S.D. Rosen, HSulf-2, an extracellular endoglycosamine-6-sulfatase, selectively mobilizes heparin-bound growth factors and chemokines: effects on VEGF, FGF-1, and SDF-1, *BMC Biochem.* 7 (2006) 1–13, <https://doi.org/10.1186/1471-2091-7-2>.
- [24] X. Yin, J. Truty, R. Lawrence, S.C. Johns, R.S. Srinivasan, T.M. Handel, M. M. Fuster, A critical role for lymphatic endothelial heparan sulfate in lymph node metastasis, *Mol. Canc.* 9 (2010) 1–20, <https://doi.org/10.1186/1476-4599-9-316>.
- [25] M. Bajénoff, J.G. Egen, L.Y. Koo, J.P. Laugier, F. Brau, N. Glaichenhaus, R. N. Germain, Stromal cell networks regulate lymphocyte entry, migration, and territoriality in lymph nodes, *Immunity* 25 (2006) 989–1001, <https://doi.org/10.1016/j.immuni.2006.10.011>.
- [26] K. Flanagan, D. Moroziewicz, H. Kwak, H. Hörig, H.L. Kaufman, The lymphoid chemokine CCL21 costimulates naïve T cell expansion and Th1 polarization of non-regulatory CD4+ T cells, *Cell. Immunol.* 231 (2004) 75–84, <https://doi.org/10.1016/j.cellimm.2004.12.006>.
- [27] A.S. Hoffman, Hydrogels for biomedical applications, *Adv. Drug Deliv. Rev.* 64 (2012) 18–23, <https://doi.org/10.1016/j.addr.2012.09.010>.
- [28] G.D. Nicodemus, S.J. Bryant, Cell encapsulation in biodegradable hydrogels for tissue engineering applications, *Tissue Eng. B Rev.* 14 (2008) 149–165, <https://doi.org/10.1089/ten.teb.2007.0332>.
- [29] A. Raic, L. Rödlig, H. Kalbacher, C. Lee-Thedieck, Biomimetic macroporous PEG hydrogels as 3D scaffolds for the multiplication of human hematopoietic stem and progenitor cells, *Biomaterials* 35 (2014) 929–940, <https://doi.org/10.1016/j.biomaterials.2013.10.038>.
- [30] S.R. Caliari, J.A. Burdick, A practical guide to hydrogels for cell culture, *Nat. Methods* 13 (2016) 405–414, <https://doi.org/10.1038/nmeth.3839>.
- [31] U. Freudenberg, Y. Liang, K.L. Kiick, C. Werner, Glycosaminoglycan-based biohybrid hydrogels: a sweet and smart choice for multifunctional biomaterials, *Adv. Mater.* 28 (2016) 8861–8891, <https://doi.org/10.1002/adma.201601908>.
- [32] D. Aydin, I. Louban, N. Perschmann, J. Bluemmel, T. Lohmueller, E.A. Cavalcanti-Adam, T.L. Haas, H. Walczak, H. Kessler, R. Fiammengo, J.P. Spatz, Polymeric substrates with tunable elasticity and nanoscopically controlled biomolecule presentation, *Langmuir* 26 (2010) 15472–15480, <https://doi.org/10.1021/la103065x>.

- [33] S.J. Bryant, K.S. Anseth, Hydrogel properties influence ECM production by chondrocytes photoencapsulated in poly(ethylene glycol) hydrogels, *J. Biomed. Mater. Res.* 59 (2002) 63–72, <https://doi.org/10.1002/jbm.1217>.
- [34] M.W. Tibbitt, K.S. Anseth, Hydrogels as extracellular matrix mimics for 3D cell culture, *Biotechnol. Bioeng.* 103 (2009) 655–663, <https://doi.org/10.1002/bit.22361>.
- [35] J. Guasch, J. Diemer, H. Riahinezhad, S. Neubauer, H. Kessler, J.P. Spatz, Synthesis of binary nanopatterns on hydrogels for initiating cellular responses, *Chem. Mater.* 28 (2016) 1806–1815, <https://doi.org/10.1021/acs.chemmater.5b04910>.
- [36] J. Zhu, Bioactive modification of poly(ethylene glycol) hydrogels for tissue engineering, *Biomaterials* 31 (2010) 4639–4656, <https://doi.org/10.1016/j.biomaterials.2010.02.044>.
- [37] H. Wang, L. Cai, A. Paul, A. Enejder, S.C. Heilshorn, Hybrid elastin-like polypeptide–polyethylene glycol (ELP-PEG) hydrogels with improved transparency and independent control of matrix mechanics and cell ligand density, *Biomacromolecules* 15 (2014) 3421–3428, <https://doi.org/10.1021/bm500969d>.
- [38] M.C. Cushing, K.S. Anseth, Hydrogel cell cultures, *Science* 316 (2007) 1133–1134, <https://doi.org/10.1126/science.1140171>.
- [39] C.T. Huynh, F. Liu, Y. Cheng, K.A. Coughlin, E. Alsborg, Thiol–epoxy “click” chemistry to engineer cyocompatible PEG-based hydrogel for siRNA-mediated osteogenesis of hMSCs, *ACS Appl. Mater. Interfaces* 10 (2018) 25936–25942, <https://doi.org/10.1021/acsami.8b07167>.
- [40] S.J. Paluck, T.H. Nguyen, H.D. Maynard, Heparin-mimicking polymers: synthesis and biological applications, *Biomacromolecules* 17 (2016) 3417–3440, <https://doi.org/10.1021/acsbiomac.6b01147>.
- [41] B. Mullooy, J. Hogwood, E. Gray, R. Lever, C.P. Page, Pharmacology of heparin and related drugs, *Pharmacol. Rev.* 68 (2016) 76–141, <https://doi.org/10.1124/pr.115.011247>.
- [42] T. Yang, A. Hussain, S. Bai, I.A. Khalil, H. Harashima, F. Ahsan, Positively charged polyethylenimines enhance nasal absorption of the negatively charged drug, low molecular weight heparin, *J. Contr. Release* 115 (2006) 289–297, <https://doi.org/10.1016/j.jconrel.2006.08.015>.
- [43] M.C.Z. Meneghetti, A.J. Hughes, T.R. Rudd, H.B. Nader, A.K. Powell, E.A. Yates, M. A. Lima, Heparan sulfate and heparin interactions with proteins, *J. R. Soc. Interface* 12 (2015) 20150589, <https://doi.org/10.1098/rsif.2015.0589>.
- [44] G.J. Merli, J.B. Groce, Pharmacological and clinical differences between low-molecular-weight heparins: implications for prescribing practice and therapeutic interchange, *P T* 35 (2010) 95–105. <https://pubmed.ncbi.nlm.nih.gov/20221326/>.
- [45] R. Sasisekharan, K. Viswanathan, Functional glycomics and the future of glycomic drugs, in: S. Ekins, J.J. Xu (Eds.), *Drug Efficacy, Safety, and Biologics Discovery*, John Wiley & Sons, Inc., New Jersey, USA, 2008, pp. 277–300.
- [46] K. Chandarajoti, J. Liu, R. Pawlinski, The design and synthesis of new synthetic low-molecular-weight heparins, *J. Thromb. Haemostasis* 14 (2016) 1135–1145, <https://doi.org/10.1111/jth.13312>.
- [47] A.D. Baldwin, K.G. Robinson, J.L. Militar, C.D. Derby, K.L. Kiick, R.E. Akins Jr., In situ crosslinkable heparin-containing poly(ethylene glycol) hydrogels for sustained anticoagulant release, *J. Biomed. Mater. Res. Part A* 100A (2012) 2106–2118, <https://doi.org/10.1002/jbm.a.34050>.
- [48] A.D. Baldwin, K.L. Kiick, Reversible maleimide–thiol adducts yield glutathione-sensitive poly(ethylene glycol)–heparin hydrogels, *Polym. Chem.* 4 (2013) 133–143, <https://doi.org/10.1039/C2PY20576A>.
- [49] N. Davydova, X.R. Rodriguez, C. Blázquez, A. Gómez, I. Perevyazko, J. Guasch, V. Sergeev, E. Laukhina, I. Ratera, J. Veciana, Functionalization of polyacrylamide for nanotrapping positively charged biomolecules, *RSC Adv.* 9 (2019) 15402–15409, <https://doi.org/10.1039/C8RA07764A>.
- [50] J.M. Zuidema, C.J. Rivet, R.J. Gilbert, F.A. Morrison, A protocol for rheological characterization of hydrogels for tissue engineering strategies, *J. Biomed. Mater. Res. Part B* 102 (2014) 1063–1073, <https://doi.org/10.1002/jbm.b.33088>.
- [51] A.N. Stachowiak, D.J. Irvine, Inverse opal hydrogel–collagen composite scaffolds as a supportive microenvironment for immune cell migration, *J. Biomed. Mater. Res. Part A* 85 (2008) 815–828, <https://doi.org/10.1002/jbm.a.31661>.
- [52] A. Ortega-Carrion, M. Vicente-Manzanares, Concerning immune synapses: a spatiotemporal timeline, *F1000Res* 5 (2016), <https://doi.org/10.12688/f1000research.7796.1>. F1000 Faculty Rev-418.
- [53] S. Stoll, J. Delon, T.M. Brotz, R.N. Germain, Dynamic imaging of T cell–dendritic cell interactions in lymph nodes, *Science* 296 (2002) 1873–1876, <https://doi.org/10.1126/science.1071065>.
- [54] M. Gunzer, A. Schäfer, S. Borgmann, S. Grabbe, K.S. Zänker, E.B. Bröcker, E. Kämpgen, P. Friedl, Antigen presentation in extracellular matrix: interactions of T cells with dendritic cells are dynamic, short lived, and sequential, *Immunity* 13 (2000) 323–332, [https://doi.org/10.1016/s1074-7613\(00\)00032-00037](https://doi.org/10.1016/s1074-7613(00)00032-00037).
- [55] M.J. Miller, S.H. Wei, I. Parker, M.D. Cahalan, Two-photon imaging of lymphocyte motility and antigen response in intact lymph node, *Science* 296 (2002) 1869–1873, <https://doi.org/10.1126/science.1070051>.
- [56] S. Adutler-Lieber, I. Zaretsky, H. Sabany, E. Kartvelishvily, O. Golani, B. Geiger, N. Friedman, Substrate-bound CCL21 and ICAM1 combined with soluble IL-6 collectively augment the expansion of antigen-specific murine CD4(+) T cells, *Blood Adv* 1 (2017) 1016–1030, <https://doi.org/10.1182/bloodadvances.2016001545>.
- [57] A.B. Suraiya, M.L. Hun, V.X. Truong, J.S. Forsythe, A.P. Chidgey, Gelatin-based 3D microgels for in vitro T lineage cell generation, *ACS Biomater. Sci. Eng.* 6 (2020) 2198–2208, <https://doi.org/10.1021/acsbiomaterials.9b01610>.
- [58] Y. Liang, K.L. Kiick, Heparin-functionalized polymeric biomaterials in tissue engineering and drug delivery applications, *Acta Biomater.* 10 (2014) 1588–1600, <https://doi.org/10.1016/j.actbio.2013.07.031>.
- [59] I. Capila, R.J. Linhardt, Heparin–protein interactions, *Angew. Chem. Int.* 41 (2002) 390–412, [https://doi.org/10.1002/1521-3773\(20020201\)41:3<390::Aid-Anie390>3.0.Co;2-b](https://doi.org/10.1002/1521-3773(20020201)41:3<390::Aid-Anie390>3.0.Co;2-b).
- [60] C. Tourasse, J.F. Dénier, A. Awada, A.-C. Gratadour, K. Nessah-Bousquet, J. Gay, Elastography in the assessment of sentinel lymph nodes prior to dissection, *Eur. J. Radiol.* 81 (2012) 3154–3159, <https://doi.org/10.1016/j.ejrad.2012.04.031>.
- [61] F. Kilic, M. Velideodeglu, T. Ozturk, S.G. Kandemirli, A.S. Dikici, M.E. Er, F. Aydogan, F. Kantarci, M.H. Yilmaz, Ex vivo assessment of sentinel lymph nodes in breast cancer using shear wave elastography, *J. Ultrasound Med.* 35 (2016) 271, <https://doi.org/10.7863/ultra.15.03039>.
- [62] S.J. Bae, J.T. Park, A.Y. Park, J.H. Youk, J.W. Lim, H.W. Lee, H.M. Lee, S.G. Ahn, E. J. Son, J. Jeong, Ex vivo shear-wave elastography of axillary lymph nodes to predict nodal metastasis in patients with primary breast cancer, *J. Breast Cancer* 21 (2018) 190–196, <https://doi.org/10.4048/jbc.2018.21.2.190>.
- [63] J. You, J. Chen, F. Xiang, Y. Song, S. Khamis, C. Lu, Q. Lv, Y. Zhang, M. Xie, The value of quantitative shear wave elastography in differentiating the cervical lymph nodes in patients with thyroid nodules, *J. Med. Ultrason.* 45 (2018) 251–259, <https://doi.org/10.1007/s10396-017-0819-0>.
- [64] J. Borst, T. Ahrends, N. Babała, C.J.M. Melief, W. Kastenmüller, CD4+ T cell help in cancer immunology and immunotherapy, *Nat. Rev. Immunol.* 18 (2018) 635–647, <https://doi.org/10.1038/s41577-018-0044-0>.
- [65] C.J. Turtle, L.-A. Hanafi, C. Berger, M. Hudecek, B. Pender, E. Robinson, R. Hawkins, C. Chaney, S. Cherian, X. Chen, L. Soma, B. Wood, D. Li, S. Heimfeld, S.R. Riddell, D.G. Maloney, Immunotherapy of non-Hodgkin lymphoma with a defined ratio of CD8(+) and CD4(+) CD19-specific chimeric antigen receptor-modified T cells, *Sci. Transl. Med.* 8 (2016) 355ra116, <https://doi.org/10.1126/scitranslmed.aaf8621>.
- [66] C.J. Turtle, L.-A. Hanafi, C. Berger, T.A. Gooley, S. Cherian, M. Hudecek, D. Sommermeyer, K. Melville, B. Pender, T.M. Budiarto, E. Robinson, N. Steevens, C. Chaney, L. Soma, X. Chen, C. Yeung, B. Wood, D. Li, J. Cao, S. Heimfeld, M.C. Jensen, S.R. Riddell, D.G. Maloney, CD19 CAR-T cells of defined CD4+:CD8+ composition in adult B cell ALL patients, *J. Clin. Invest.* 126 (2016) 2123–2138, <https://doi.org/10.1172/JCI85309>.
- [67] D. Sommermeyer, M. Hudecek, P.L. Kosasih, T. Gogishvili, D.G. Maloney, C. J. Turtle, S.R. Riddell, Chimeric antigen receptor-modified T cells derived from defined CD8- and CD4+ subsets confer superior antitumor reactivity in vivo, *Leukemia* 30 (2015) 492–500, <https://doi.org/10.1038/leu.2015.247>.
- [68] E. Tran, S. Turcotte, A. Gros, P.F. Robbins, Y.-C. Lu, M.E. Dudley, J.R. Wunderlich, R.P. Somerville, K. Hogan, C.S. Hinrichs, M.R. Parkhurst, J.C. Yang, S. A. Rosenberg, Cancer immunotherapy based on mutation-specific CD4+ T cells in a patient with epithelial cancer, *Science* 344 (2014) 641–645, <https://doi.org/10.1126/science.1251102>.
- [69] E.M. Inderberg, S. Wälchli, Long-term surviving cancer patients as a source of therapeutic TCR, *Cancer Immunology, Immunotherapy* 69 (2020) 859–865, <https://doi.org/10.1007/s00262-019-02468-9>.
- [70] A.B. Lyons, C.R. Parish, Determination of lymphocyte division by flow cytometry, *J. Immunol. Methods* 171 (1994) 131–137, [https://doi.org/10.1016/0022-1759\(94\)90236-4](https://doi.org/10.1016/0022-1759(94)90236-4).
- [71] Y. Xue, X. Li, H. Li, W. Zhang, Quantifying thiol–gold interactions towards the efficient strength control, *Nat. Commun.* 5 (2014) 4348, <https://doi.org/10.1038/ncomms5348>.
- [72] E. Ziegler, M. Oberbarnscheidt, S. Bülfone-Paus, R. Förster, U. Kunzendorf, S. Krautwald, CCYR signaling inhibits T cell proliferation, *J. Immunol.* 179 (2007) 6485–6493, <https://doi.org/10.4049/jimmunol.179.10.6485>.
- [73] M. Roederer, Interpretation of cellular proliferation data: avoid the panglossian, *Cytometry A* 79A (2011) 95–101, <https://doi.org/10.1002/cyto.a.21010>.
- [74] A.L. Garfall, E.K. Dancy, A.D. Cohen, W.-T. Hwang, J.A. Fraietta, M.M. Davis, B. L. Levine, D.L. Siegel, E.A. Stadtmauer, D.T. Vogl, A. Waxman, A.P. Rapoport, M. C. Milone, C.H. June, J.J. Melenhorst, T-cell phenotypes associated with effective CAR T-cell therapy in postinduction vs relapsed multiple myeloma, *Blood Adv* 3 (2019) 2812–2815, <https://doi.org/10.1182/bloodadvances.2019000600>.
- [75] E. Scibona, M. Morbidelli, Expansion processes for cell-based therapies, *Biotechnol. Adv.* 37 (2019) 107455, <https://doi.org/10.1016/j.biotechadv.2019.107455>.
- [76] T. Ushiki, O. Ohtani, K. Abe, Scanning electron microscopic studies of reticular framework in the rat mesenteric lymph node, *Anat. Rec.* 241 (1995) 113–122, <https://doi.org/10.1002/ar.1092410115>.
- [77] K. Shen, V.K. Thomas, M.L. Dustin, L.C. Kam, Micropatterning of costimulatory ligands enhances CD4+ T cell function, *Proc. Natl. Acad. Sci. U. S. A* 105 (2008) 7791–7796, <https://doi.org/10.1073/pnas.0710295105>.
- [78] G.A.V. Seventer, Y. Shimizu, K.J. Hogan, S. Shaw, The LFA-1 ligand ICAM-1 provides an important costimulatory signal for T cell receptor-mediated activation of resting T cells, *J. Immunol.* 144 (1990) 4579–4586. <https://www.ncbi.nlm.nih.gov/pubmed/1972160>.
- [79] J.W. Hickey, Y. Dong, J.W. Chung, S.F. Salathe, H.C. Pruitt, X. Li, C. Chang, A. K. Fraser, C.A. Bessell, A.J. Ewald, S. Gerecht, H.-Q. Mao, J.P. Schneck, Engineering an artificial T-cell stimulating matrix for immunotherapy, *Adv. Mater.* 31 (2019) 1807359, <https://doi.org/10.1002/adma.201807359>.
- [80] C.S. Hinrichs, Z.A. Borman, L. Gattinoni, Z. Yu, W.R. Burns, J. Huang, C. Klebanoff, L.A. Johnson, S.P. Kerkar, S. Yang, P. Muranski, D.C. Palmer, C. D. Scott, R.A. Morgan, P.F. Robbins, S.A. Rosenberg, N.P. Restifo, Human effector CD8+ T cells derived from naive rather than memory subsets possess superior traits for adoptive immunotherapy, *Blood* 117 (2011) 808–814, <https://doi.org/10.1182/blood-2010-05-286286>.
- [81] J. Zhu, H. Yamane, W.E. Paul, Differentiation of effector CD4 T cell populations, *Annu. Rev. Immunol.* 28 (2010) 445–489, <https://doi.org/10.1146/annurev-immunol-030409-101212>.

- [82] L. Gattinoni, C.A. Klebanoff, D.C. Palmer, C. Wrzesinski, K. Kerstann, Z. Yu, S. E. Finkelstein, M.R. Theoret, S.A. Rosenberg, N.P. Restifo, Acquisition of full effector function in vitro paradoxically impairs the *in vivo* antitumor efficacy of adoptively transferred CD8+ T cells, *J. Clin. Invest.* 115 (2005) 1616–1626, <https://doi.org/10.1172/JCI200318007>.
- [83] M.E. Pipkin, J.A. Sacks, F. Cruz-Guilloty, M.G. Lichtenheld, M.J. Bevan, A. Rao, Interleukin-2 and inflammation induce distinct transcriptional programs that promote the differentiation of effector cytolytic T cells, *Immunity* 32 (2010) 79–90, <https://doi.org/10.1016/j.immuni.2009.11.012>.
- [84] J. Weiden, D. Voerman, Y. Dölen, R.K. Das, A.v Duffelen, R. Hammink, L. Eggermont, A.E. Rowan, J. Tel, C.G. Figdor, Injectable biomimetic hydrogels as tools for efficient T cell expansion and delivery, *Front. Immunol.* 9 (2018) 2798, <https://doi.org/10.3389/fimmu.2018.02798>.
- [85] U. Unzueta, M.V. Céspedes, N. Ferrer-Miralles, I. Casanova, J. Cedano, J. L. Corchero, J. Domingo-Espín, A. Villaverde, R. Mangues, E. Vázquez, Intracellular CXCR4+ cell targeting with T22-empowered protein-only nanoparticles, *Int. J. Nanomed.* 7 (2012) 4533–4544, <https://doi.org/10.2147/IJN.S34450>.
- [86] T. Nie, R.E. Akins, K.L. Kiick, Production of heparin-containing hydrogels for modulating cell responses, *Acta Biomater.* 5 (2009) 865–875, <https://doi.org/10.1016/j.actbio.2008.12.004>.
- [87] T. Nie, A. Baldwin, N. Yamaguchi, K.L. Kiick, Production of heparin-functionalized hydrogels for the development of responsive and controlled growth factor delivery systems, *J. Control. Release* 122 (2007) 287–296, <https://doi.org/10.1016/j.jconrel.2007.04.019>.